Numerical methods for probing complex objects

Hélène Barucq[1].

[1]Project-Team Makutu, Inria–TotalEnergies–UPPA, LMAP, UMR CNRS 5142

Table of Contents

Plan

1. Introduction

Broad scientific context

Describe a place with exactness from more or less numerous and precise memories, or guessing the content and internal structures of an object after having observed it only partially, without ever touching it because it is inaccessible or very fragile?

1. **Wave propagation is helping**
2. **Waves are very sensitive to any change in the propagation medium.**

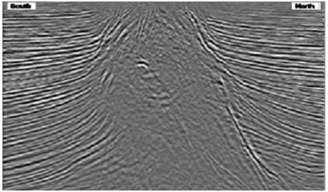

(a) Seismogram.

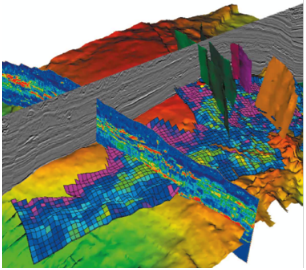

(b) Reservoir model.

Inverse problems

Basically, inverse wave problems are composed of:

1. Emitting sources that will propagate through the medium and recording the reflected waves on a set of receivers; acquisition/ forward problem
2. From the acquisitions, find the propagation medium; inverse problem/backward problem

Example: Seismic imaging for the **Reconstruction/Monitoring** of subsurface Earth properties

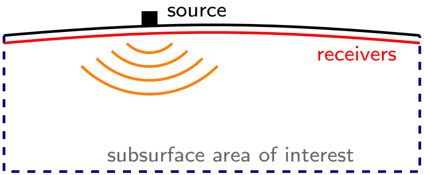

1. **Accurate simulation of wave propagation in large-scale complex media,**
2. **Efficient procedure for nonlinear reconstruction of properties.**

Numerical data match real data

Compare data with simulations: computationally and possibly timely expensive

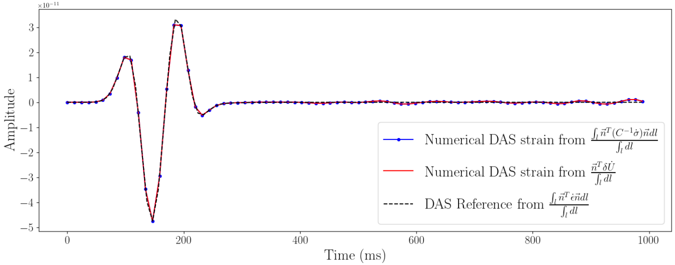

Comparison of observation and numerical result

..

Example: access to energy resources

- Hydrocarbons
- Geothermal
- Hydrogen

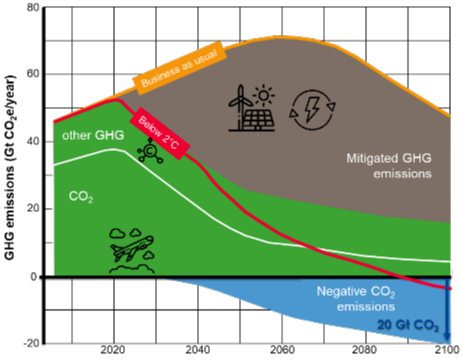

Source: The Emissions Gap Report 2017. United Nations Environment Programme (UNEP)

Facilitate safe carbon capture, utilization and storage - CCUS

- CO2 emissions: leading cause of climate change;
- Geological storage of CO2: important tool for the stabilization of atmospheric greenhouse gas concentrations;
- CO2 is injected into underground geological formations; Safe, permanent, and effective.

How do we ensure the safety and sustainability of storage?

That's where seismic monitoring comes into play.

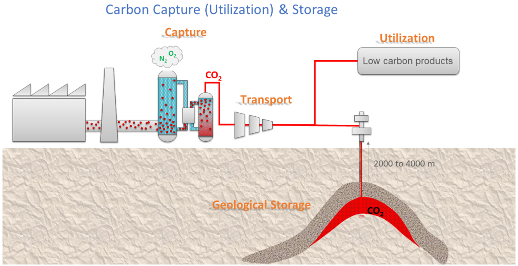

Research routine: propagation domains

- 3D large domains
- topography, heterogeneity
- a network of sources whose number is of the order of several thousands

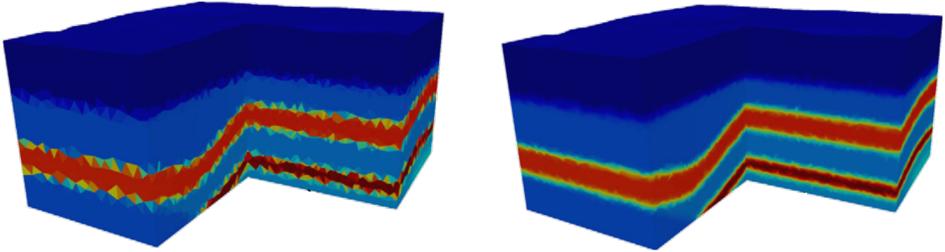

Parameterization matters

Research routine: wave equations, see Arjeta Heta Poster!

- Acoustic wave equation,
- Elastic wave equation,
- Electromagnetic wave equation,
- Couplings

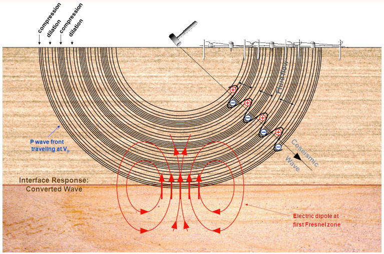

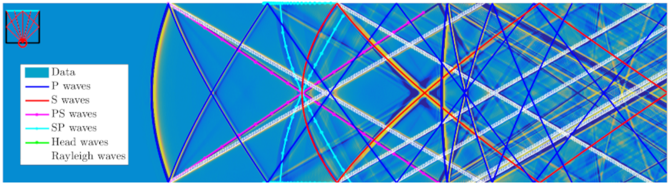

Waves in solid media

Equations 2/2

Acoustic wave equation, time and frequency domains:

$$\begin{cases} \rho\partial_t \mathbf{v}(\mathbf{x},t) = -\nabla p(\mathbf{x},t), \\ \dfrac{1}{c^2\rho}\partial_t p(\mathbf{x},t) + \boldsymbol{\nabla}\cdot\mathbf{v}(\mathbf{x},t) = 0. \end{cases}$$

$$\begin{cases} -\mathrm{i}\,\omega\rho\mathbf{v}(\mathbf{x},\omega) = -\nabla p(\mathbf{x},\omega), \\ -\dfrac{1}{c^2\rho}\mathrm{i}\omega p(\mathbf{x},\omega) + \boldsymbol{\nabla}\cdot\mathbf{v}(\mathbf{x},\omega) = 0. \end{cases}$$

Elasto-dynamic equations, time and frequency domains:

$$\begin{cases} \rho\partial_t \mathbf{v}(\mathbf{x},t) = \boldsymbol{\nabla}\cdot\underline{\underline{\sigma}}(\mathbf{x},t), \\ \partial_t\underline{\underline{\sigma}}(\mathbf{x},t) = \underline{\underline{C}}(\mathbf{x})(\underline{\underline{\epsilon}}(\mathbf{v})). \end{cases}$$

$$\begin{cases} -\mathrm{i}\omega\rho\mathbf{v}(\mathbf{x},\omega) = \boldsymbol{\nabla}\cdot\underline{\underline{\sigma}}(\mathbf{x},\omega), \\ -\mathrm{i}\omega\underline{\underline{\sigma}}(\mathbf{x},\omega) = \underline{\underline{C}}(\mathbf{x})(\underline{\underline{\epsilon}}(\mathbf{v})). \end{cases}$$

Equations 2/2

Each approach has pros and cons

Time-domain formulation

- Using data is straightforward
- Matrix-free implementation relieves memory,
- frequency-dependent parameters,
- adjoint of the discrete problem can differ from discrete adjoint, additional developments are required,
- multi-sources

Time-harmonic formulation

- Easily handle attenuation,
- multi-sources with direct solver,
- reuse matrix factorization for adjoint-problem in inversion,
- memory cost for matrix factorization with direct solver,

Modelling and simulation challenges 1/2

A multi-physics problem and...

- ✓ $CO2$ sequestration and monitoring are more and more recognized as a key element in the path towards energy decarbonization
- ✓ $CO2$ sequestration and monitoring is an excellent example gathering the leading-edge technology of many different domain to help in the prediction of the plume evolution:
  - ✓ Flow and geo-mechanical simulation,
  - ✓ Gravimetry,
  - ✓ Seismic modelling and inverse problem, monitoring acquisition technology,
  - ✓ In situ data visualization and analysis,
  - ✓ Machine learning
  - ✓ ...

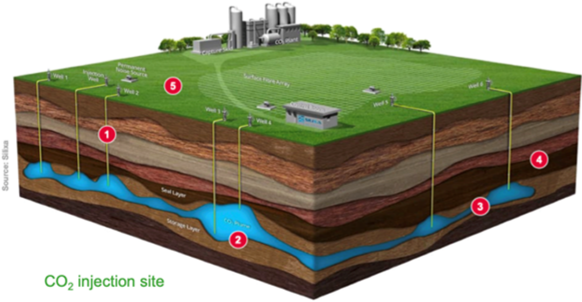

CO_2 injection site

1. Well integrity/injectivity
2. Pressure/Stress change, Fault Activation
3. CO_2 transport & trapping
4. Seal integrity
5. Surface deformation, Seismicity

Modelling and simulation challenges 2/2

HPC Issue

- ✓ **Limitations:**
  - ✓ **Multiphysics: geomechanic+Flow+Seismic**
  - ✓ **Large Scale: 98% storage in Aquifer**
  - ✓ **Long Term Simulation: post injection matters**
- ✓ **Solutions:**
  - ✓ **Fast and scalable algorithms**
  - ✓ **Perennial solutions: portability**

Target: Exascale Computers

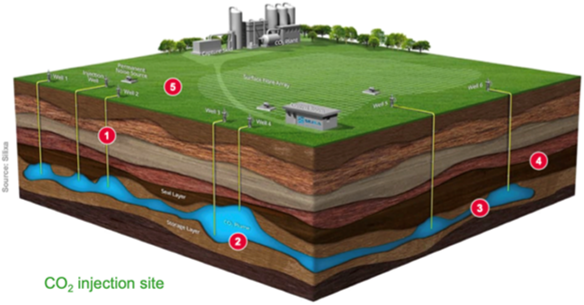

CO_2 injection site

1. Well integrity/injectivity
2. Pressure/Stress change, Fault Activation
3. CO_2 transport & trapping
4. Seal integrity
5. Surface deformation, Seismicity

Numerical methods 1/2

- Finite Differences: implementation easy, low cost, inaccuracy for the topography
- Finite Elements: implementation possibly tricky, expensive, accurate for the topography
- Boundary integral equations: not efficient in highly heterogeneous media
- Semi-Analytical: lack of flexibility, geometrical effects, anisotropy neglected,

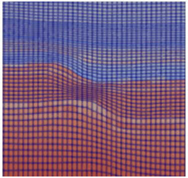

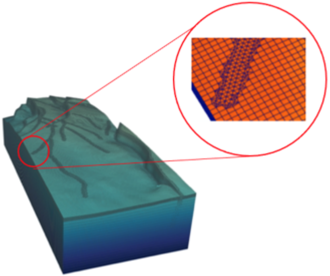

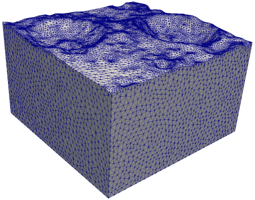

In Makutu team 2/2

- Spectral element methods (SEM)
- Discontinuous Galerkin methods (DG)
- Non polynomial basis functions in Trefftz framework

- Explicit schemes in time
- High-order
- hp-adaptivity with DG

GEOSX

Multiphysics
Simulator on HPC

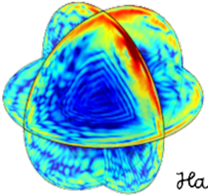

Hawen

https://ffaucher.gitlab.io/hawen-website/

Plan

2. Analytical solutions: numerical methods are needed

1D acoustic wave equation

Let c be the velocity supposed to be constant, we consider

$$\frac{1}{c^2}\partial_t^2 u(x,t) - \partial_x^2 u(x,t) = f(\mathbf{x},t), \qquad \text{for } x \in \mathbb{R} \text{ and } t \geq 0 \tag{1}$$

with a source term $f \in \mathcal{D}(\mathbb{R} \times \mathbb{R}_+)$, and initial conditions

$$u(x,0) = u_0(x) \quad \text{and} \quad \partial_t u(x,0) = u_1(x) \quad \text{for } x \in \mathbb{R}, u_0 \text{ and } u_1 \in \mathcal{D}(\mathbb{R}). \tag{2}$$

Let X and Y be defined as:

$$\begin{cases} X = x + ct \\ Y = x - ct \end{cases}. \tag{3}$$

Introduce fields in the new coordinate system:

$$U(X,Y) \;=\; u(x,t) \quad \text{and} \quad F(X,Y) \;=\; f(x,t). \tag{4}$$

Integrate along the characteristics

From the chain rule, we have

$$\frac{\partial u}{\partial x}(x,t) \;=\; \frac{\partial X}{\partial x}\frac{\partial U}{\partial X}(X,Y) \;+\; \frac{\partial Y}{\partial x}\frac{\partial U}{\partial Y}(X,Y) \;=\; \Big(\frac{\partial}{\partial X} \;+\; \frac{\partial}{\partial Y}\Big)U(X,Y). \tag{5}$$

By repeating the same reasoning, we get

$$\frac{\partial^2 u}{\partial x^2}(x,t) \;=\; \Big(\frac{\partial}{\partial X} + \frac{\partial}{\partial Y}\Big)^2 U(X,Y). \tag{6}$$

and

$$\frac{\partial^2 u}{\partial t^2}(x,t) \;=\; c^2 \Big(\frac{\partial}{\partial X} - \frac{\partial}{\partial Y}\Big)^2 u(x,t). \tag{7}$$

In the new coordinate system, the wave equation reads:

$$\Big(\frac{\partial}{\partial X} - \frac{\partial}{\partial Y}\Big)^2 U(X,Y) - \Big(\frac{\partial}{\partial X} + \frac{\partial}{\partial Y}\Big)^2 U(X,Y) = F(X,Y), \tag{8}$$

which simplifies to

$$-4\frac{\partial^2 U}{\partial X \partial Y}(X,Y) = F(X,Y). \tag{9}$$

Case 1: $F(X, Y) = 0$

We have

$$\frac{\partial^2 U}{\partial X \partial Y}(X, Y) = 0. \tag{10}$$

The function $\dfrac{\partial U}{\partial Y}$ is a constant with respect to X:

$$\frac{\partial U}{\partial Y}(X, Y) = w(Y). \tag{11}$$

If u_+ is a primitive of w, function $U(X, Y)$ is given by

$$U(X, Y) = u_+(Y) + u_-(X). \tag{12}$$

with u_- a function of X. Therefore, u reads:

$$u(x, t) = u_-(x - ct) + u_+(x + ct). \tag{13}$$

u_+ moves to the right with velocity c, u_- moves to the left with velocity c.

Illustration

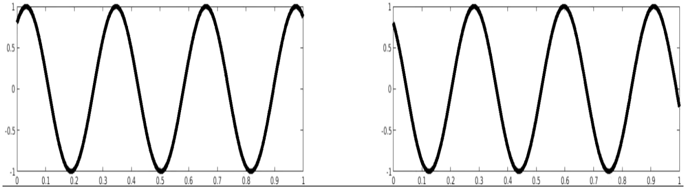

Case 1: F(X,Y)=0

To determine u_+ and u_-, we use the boundary conditions

$$u_+(x) + u_-(x) = u_0(x) \quad \text{and} \quad -cu'_+(x) + cu'_-(x) = u_1(x). \tag{14}$$

By integrating the second equality, we have

$$-cu_+(x) + cu_-(x) = \int_{-\infty}^{x} u_1(s)ds + C \tag{15}$$

where C is a constant. Then using (14) we get

$$u(x,t) = \frac{u_0(x-ct)}{2} + \frac{u_0(x+ct)}{2} + \frac{1}{2c}\int_{x-ct}^{x+ct} u_1(s)ds. \tag{16}$$

Case 2: $u_0(\mathbf{x}) = 0$ and $u_1(\mathbf{x}) = 0$

In the new set of variables, the initial conditions are written for all $Z \in \mathbb{R}$

$$U(Z,Z) = 0 \quad \text{and} \quad \frac{\partial U}{\partial X}(Z,Z) = 0 \quad \text{and} \quad \frac{\partial U}{\partial Y}(Z,Z) = 0. \tag{17}$$

Taking $X' \in \mathbb{R}$, we can then integrate (9) and get

$$\frac{\partial U}{\partial Y}(X',Y) - \frac{\partial U}{\partial Y}(Y,Y) = \int_Y^{X'} \frac{\partial^2 U}{\partial X \partial Y}(X,Y)dX = -\int_Y^{X'} \frac{F(X,Y)}{4}dX. \tag{18}$$

From (17), we get

$$\frac{\partial U}{\partial Y}(X',Y) \; = \; -\int_Y^{X'} \frac{F(X,Y)}{4}dX. \tag{19}$$

In the same way, we take $Y' \in \mathbb{R}$, and we integrate over Y

$$U(X',X') - U(X',Y') \; = \; \int_{Y'}^{X'} \frac{\partial U}{\partial Y}(X',Y)dY \; = \; -\int_{Y'}^{X'} \Big(\int_Y^{X'} \frac{F(X,Y)}{4}dX \Big) dY. \tag{20}$$

Case 2: $u_0(\mathbf{x}) = 0$ and $u_1(\mathbf{x}) = 0$

We get

$$U(X', Y') = \int_{Y'}^{X'} \Big(\int_{Y}^{X'} \frac{F(X,Y)}{4} dX \Big) dY. \tag{21}$$

We denote by $\widehat{T}_{X,Y}$ the set in $\mathbb{R}^2$ given by

$$\widehat{T}_{X',Y'} = \Big\{ (X,Y) \in \mathbb{R}^2 \,:\, Y' \leq Y \leq X \leq X' \Big\}. \tag{22}$$

We have

$$U(X', Y') = \int_{\widehat{T}_{X',Y'}} \frac{F(X,Y)}{4} dX dY. \tag{23}$$

Case 2: $u_0(\mathbf{x}) = 0$ and $u_1(\mathbf{x}) = 0$

Going back to variables (x, t), this expression becomes

$$u(x', t') = \int_{T_{x',t'}} \frac{f(x,t)}{2} dxdt \qquad (24)$$

with $T_{x',t'}$ the reciprocal image of $\widehat{T}_{X,Y}$ which is called the past cone, see figure **??**. This past cone is defined by

$$\begin{cases} T_{x',t'} &= \Big\{(x,t) \in \mathbb{R} \times \mathbb{R}^+ \ : \ x' - ct' \leq x - ct \leq x + ct \leq x' + ct'\Big\} \\ &= \Big\{(x,t) \in \mathbb{R} \times \mathbb{R}^+ \ : \ x' - c(t'-t) \leq x \leq x' + c(t'-t)\Big\}. \end{cases} \qquad (25)$$

General case

Let $T_{x,t}$ be the past cone:

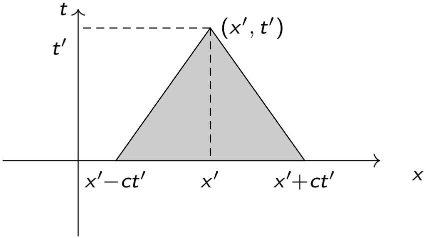

The solution to the full problem is reconstructed thanks to linearity:

Proposition

Let initial data u_0 and u_1, and volumetric source f be given. We then have:

$$u(x,t) = \frac{u_0(x-ct)}{2} + \frac{u_0(x+ct)}{2} + \frac{1}{2c}\int_{x-ct}^{x+ct} u_1(x')dx' + \int_{T_{x,t}} \frac{f(x',t')}{2} dx'dt'. \tag{26}$$

Plane waves

Let the 3D acoustic wave equation

$$\frac{\partial^2 u}{\partial t^2}(\mathbf{x}, t) - c^2 \Delta u(\mathbf{x}, t) = 0 \quad \text{for all } \mathbf{x} \in \mathbb{R}^3 \text{ and } t \in \mathbb{R}^+. \tag{27}$$

Plane waves are the solutions to (27) of the form

$$u(\mathbf{x}, t) \; = \; U \, \exp(i\omega t \pm i\mathbf{k} \cdot \mathbf{x}) \quad \text{for } \mathbf{x} \in \mathbb{R}^3 \text{ and } t \geq 0. \tag{28}$$

with the **dispersion relation**

$$\omega^2 = c^2 |\mathbf{k}|^2, \tag{29}$$

$\mathbf{k}$ is the wave vector, $k = |\mathbf{k}|$ is the wave number defined by $k = \frac{\omega}{c}$, agreeing that $k \geq 0$.

Fundamental solutions: Green function

Exact solutions can also be constructed from the Green function G that is defined for a PDE as the solution to:

$$\mathcal{L}G = \delta$$

where δ denotes the Dirac distribution. Then a solution to

$$\mathcal{L}u = f$$

reads

$$u = G * f$$

where $*$ stands for the convolution operator. Obviously it is crucial to check that the convolution is possible, I mean, f must be regular enough and the construction of G can be very difficult in complex media. I will show an example later on in the course.

Solar Green's function

Solar Green's function in axisymmetry, simulated using code Montjoie.

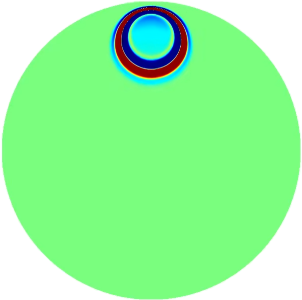

Some references

- Construction of **quasi-analytical solutions** with special functions like Bessel and Hankel functions, see Abramowitz, Milton, and Irene A. Stegun, eds. Handbook of mathematical functions with formulas, graphs, and mathematical tables. Vol. 55. US Government printing office, 1948.
- Take a look at the **Digital Library of Mathematical Functions**, https://dlmf.nist.gov/
- Quasi-analytical solutions can be **computed** for specific domains, see https://gitlab.inria.fr/jdiaz/gar6more3d. Based on **Cagniard-de-Hoop method**.
- A nice book: Nédélec, Jean-Claude. Acoustic and electromagnetic equations: integral representations for harmonic problems. Vol. 144. New York, Springer, 2001.

Plan

3 Well-posedness, that is an important question!

Maximal monotonous operator

Definition

Let H be a Hilbert space, let $<,>$ denote the scalar product on H, let A be an unbounded operator on H with domain $D(\mathrm{A})$. A is **monotonous** if $< \mathrm{Av}, \mathrm{v} > \geq 0$ for any $\mathrm{v} \in D(\mathrm{A})$. Moreover, it is **maximal** if for any F in H, there exists $\mathrm{v} \in D(\mathrm{A})$ such that $(Id + A)\mathrm{v} = \mathrm{F}$.

Example: let $H = H_0^1(\Omega) \times L^2(\Omega)$ equipped with the graph norm

$$\|(u, v)\|_H^2 = \|\nabla u\|^2 + \|v\|^2$$

Then, if

$$A = \begin{pmatrix} 0 & 1 \\ -\Delta & 0 \end{pmatrix}$$

we have:

$$D(A) = \{(u, v) \in H, A(u, v) \in H\}$$

and for any $(u, v) \in D(A)$,

$$< A(u, v), (u, v) >_H = 0$$

Hille-Yosida theorem

- Powerful and fundamental tool of the semi-group theory
- Linking the energy dissipation properties of an unbounded operator A with domain $D(A)$ to the existence, uniqueness and regularity of solutions

Theorem (Hille-Yosida)

Let H *be a Hilbert space,* $\mathrm{f} \in C^1([0,+\infty[,\mathrm{H})$ *and* $\mathrm{A} : D(\mathrm{A}) \subset \mathrm{H} \longrightarrow \mathrm{H}$ *be a maximal monotone unbounded operator,* $\mathrm{u}_0 \in D(\mathrm{A})$*. The following problem:*

$$\begin{cases} \textit{Find } \mathrm{u} \textit{ such that} \\ \dfrac{d\mathrm{u}}{dt}(t) + \mathrm{A}\mathrm{u}(t) = \mathrm{f}(t) \quad \forall t \geq 0 \quad \textit{and} \quad \mathrm{u}(0) = \mathrm{u}_0. \end{cases} \tag{30}$$

has a unique solution u *and* $\mathrm{u} \in C^1([0,+\infty[,\mathrm{H}) \cap C^0([0,+\infty[,D(\mathrm{A}))$

Fredholm alternative 1/3

Theorem (Linear Algebra)

If V *is an n-dimensional vector space and* $\mathrm{T} : \mathrm{V} \to \mathrm{V}$ *is a linear transformation, then exactly one of the following holds:*

- *For each vector* v *in* V *there is a vector* u *in* V *so that* $\mathrm{T}(\mathrm{u}) = \mathrm{v}$. *In other words:* T *is surjective*
- *dim ker* $\mathrm{T} \geq 0$.

Observe that since V is finite dimensional, if T is surjective, then it is injective.

Theorem (Solving elliptic boundary value problem)

Let V *be a Banach space, let* T *be a compact operator in* V. *Then exactly one of the following holds: let* $\lambda \in \mathbf{C}$

- $T\mathrm{v} - \lambda x \mathrm{v} = 0$ *has a non zero solution.*
- $Tx - \lambda x = \mathrm{v}$ *has a unique solution for any* $\mathrm{v} \in \mathrm{V}$.

Fredholm alternative 2/3

For instance, T is an integral operator with a smooth integral kernel.
Remark: any nonzero λ which is not an eigenvalue of a compact operator is in the resolvent, i.e., $(T - \lambda I)^(- 1)$, is bounded. The basic special case is when V is finite-dimensional, in which case any non-degenerate matrix is diagonalizable.

Fredholm alternative 3/3

Example: let f be given in $L^2(\Omega)$, with Ω a bounded regular domain. We consider the problem: find u in $H_0^1(\Omega)$ satisfying

$$\Delta u + \lambda u = f \in \Omega$$

. Then,

- If $\Re\lambda \leq 0$, u exists and is unique; the problem is strongly elliptic and Lax-Milgram theorem applies.
- If $\Re\lambda \geq 0$, we apply the Fredholm alternative by observing that the problem rewrites as $Tu = \lambda_0 u + f$ with $\lambda_0 \in \mathbf{R}$ with $\Re\lambda - \lambda_0 \leq 0$. Then T is a compact perturbation of Identity thanks to compact injections of Sobolev spaces.

Plan

4 Waves in unbounded domains

Absorbing boundary conditions in 1D 1/3

We consider the equation

$$\begin{cases} \partial_t^2 u(x,t) - \partial_x^2 u(x,t) = f(x,t) \text{ for } x \in \mathbb{R} \text{ and } t \geq 0, \\ u(x,0) = u_0(x) \quad \partial_t u(x,0) = u_1(x) \text{ for } x \in \mathbb{R}. \end{cases} \tag{31}$$

whose source term $f : \mathbb{R}_+ \times \mathbb{R} \longrightarrow \mathbb{R}$, and initial conditions $u_0 : \mathbb{R}_+ \longrightarrow \mathbb{R}$ and $u_1 : \mathbb{R}_+ \longrightarrow \mathbb{R}$ are C^∞ functions whose support is included in the interval$D =]-L, L[$ with $L > 0$:

$$f(x,t) = 0, \quad u_0(x) = 0 \text{ and } u_1(x) = 0 \text{ for } x \notin D \text{ and } t \geq 0. \tag{32}$$

Absorbing boundary conditions in 1D 2/3

Outside the support of f, we have seen that the solution reads:

$$\begin{cases} u(x,t) = u_+(x-t) \text{ for } x > L, \\ u(x,t) = u_-(x+t) \text{ for } x < -L \end{cases} \tag{33}$$

Functions u_+ and u_- are C^∞ functions satisfying

$$u_+(s) = 0 \text{ for } s \geq L \quad \text{and} \quad u_-(s) = 0 \text{ for } s \leq -L. \tag{34}$$

We truncate the boundary domain at the ends of the interval, i.e. at $x = L$ and $x = -L$ and to make the problem well-posed, we add boundary conditions at the ending points. Thanks to the explicit form ((33)) of the solution, we see that

$$\begin{cases} \dfrac{\partial u}{\partial t}(L,t) + \dfrac{\partial u}{\partial x}(L,t) = 0, \\ \dfrac{\partial u}{\partial t}(-L,t) - \dfrac{\partial u}{\partial x}(-L,t) = 0. \end{cases} \tag{35}$$

Absorbing boundary conditions 3/3

We consider the boundary-value problem:

$$\begin{cases} \partial_t^2 u(x,t) - \partial_x^2 u(x,t) = f(x,t) \text{ for } x \in]-L, L[\text{and } t \geq 0, \\ u(x,0) = u_0(x), \quad \partial_t u(x,0) = u_1(x) \text{ for } x \in]-L, L[\\ \dfrac{\partial u}{\partial t}(L,t) + \dfrac{\partial u}{\partial x}(L,t) = 0, \quad \dfrac{\partial u}{\partial t}(-L,t) - \dfrac{\partial u}{\partial x}(-L,t) = 0 \text{ for } t \geq 0. \end{cases} \tag{36}$$

and the solution to this problem provides a numerical representation of the phenomenon a priori set in the free space $\mathbf{R}$ in the region $]-L, L[$. It remains, nevertheless, to prove that the regional problem (36) is well-posed. For that purpose, we apply the Hille-Yosida theorem.

ABC: Well-posedness 1/5

Let $v = \dfrac{1}{c}\partial_t u$ and $U = (u, v)^T$.

$$\begin{cases} \partial_t u(x,t) - cv(x,t) = 0 \\ \partial_t v(x,t) - c\partial_x^2 u(x,t) = f(x,t) \text{ for } x \in]-L, L[\text{ et } t \geq 0, \\ u(x,0) = u_0(x), \quad v(x,0) = \dfrac{1}{c} u_1(x) \text{ for } x \in]-L, L[\\ v(L,t) + \dfrac{\partial u}{\partial x}(L,t) = 0, \quad v(-L,t) - \dfrac{\partial u}{\partial x}(-L,t) = 0 \text{ for } t \geq 0. \end{cases} \tag{37}$$

We have

$$\frac{dU}{dt} + AU = F \tag{38}$$

with

$$A = \left(\begin{array}{c|c} 0 & c \\ c\ \partial_x^2 & 0 \end{array} \right)$$

ABC: Well-posedness 2/5

We introduce the Hilbert space $\mathrm{H} = \mathcal{H}^1(I) \times L^2(I)$ where $I = [-L, L]$. The space $\mathcal{H}^1$ denotes the Sobolev space **quotient by constants**. H is equipped with the graph norm. The domain of A is defined by:

$$D(A) = \left\{(u, v) \in H^2(I) \times H^1(I) : v(L) = -\frac{\partial u}{\partial x}(L) \text{ and } v(-L) = \frac{\partial u}{\partial x} u(-L)\right\}$$

We prove that $A + I$ is maximal monotone on H. For that purpose, we compute (AU, U) for any $U \in D(A)$. We have:

$$(AU, U)_{\mathrm{H}} = -\partial_x u(L) v(L) + \partial_x u(-L) v(-L). \tag{39}$$

Since $v(L) = -\partial_x u(L)$ and $v(-L) = \partial_x u(-L)$ we get

$$(AU, U)_H = \Big(v(L)\Big)^2 + \Big(v(-L)\Big)^2 \geq 0 \tag{40}$$

We end up with

$$((A + I)U, U)_H \geq 0 \qquad (A + I \text{ is monotone}) \tag{41}$$

ABC: Well-posedness 3/5

We continue by proving that $A + I$ is maximal. We consider the problem

$$U \in D(A) : AU + U = F \tag{42}$$

with $F = (f, g) \in H = H^1(I) \times L^2(I)$. We have:

$$\begin{cases} u \in H^2(I) \text{ and } v \in H^1(I) \\ -v + 2u = f \in H^1(I) \\ -\partial_x^2 u + v = g \in L^2(I) \\ v(L) = -\partial_x u'(L) \\ v(-L) = \partial_x(-L) \end{cases} \tag{43}$$

We can remove $v = u - f$ to simplify the system into a scalar equation

$$\begin{cases} u \in H^2(I) \\ -\partial_x^2 u + 2u = f + g \in L^2(I), \end{cases} \tag{44}$$

ABC: Well-posedness 4/5

We have a variational formulation

$$u \in H^1(I) : a(u,w) = l(w) \quad \forall w \in H^1(I) \tag{45}$$

with

$$\begin{cases} a(u,w) &= \displaystyle\int_{-L}^{L} u'(x)w'(x) + 4u(x)w(x)dx + 2u(L)w(L) + 2u(-L)w(-L) \\ l(w) &= \displaystyle\int_{-L}^{L} \Big(2f(x) + g(x)\Big)w(x)dx + f(L)w(L) + f(-L)w(L) \end{cases} \tag{46}$$

Lax-Milgram theorem allows us to conclude: problem (45) admits a unique solution.

ABC: Well-posedness 5/5

The 1D case is a very particular case since from the solution computed in the truncates domain, it is possible to plot the solution in the free space. Indeed, we have seen that

$$\begin{cases} u(x,t) = u_+(x-t) \text{ for } x > L, \\ u(x,t) = u_-(x+t) \text{ for } x < -L \end{cases} \tag{47}$$

Hence, outside $x \in [-L, L]$, $u(x,t) = 0$ if$|x| - L > ct$ and if not

$$\begin{cases} u(x,t) = u(L, t - \frac{x-L}{c}) \text{ for } x > L, \\ u(x,t) = u(-L, t + \frac{x+L}{c}) \text{ for } x < -L. \end{cases} \tag{48}$$

Unfortunately, if the ABC is exact in 1D, it is no more the case in larger dimensions. Actually, the transparent (exact) condition exists but it is a pseudo-differential operator, global both in time and space. Its localization is required for numerical purpose but there is a price to pay: the external boundary is no more transparent, the numerical solution is polluted by reflections.

Plan

5. Introduction to discontinuous Galerkin methods

Motivations

- DG variational formulations are implemented at the element level first, to be next agglomerate by summing all over the elements: conducive for massively parallel computing
- Numerical dispersion is reduced
- DG allows us to apply *hp*-adaptivity
- Conducive to coupling with other nuemrical methods (CG-DG)

Mathematical problem setting 1/2

We consider the 1D case, the domain of study is $[0, L]$ with L a positive real. The problem of interest reads:

$$\begin{cases} \text{Find } u \in H^1(0,L) \text{ and } v \in H^1(0,L) \text{ such that} & \\ \dfrac{\mathrm{d}v}{\mathrm{d}x}(x) = i\kappa u(x) + f_u(x) & \text{for } 0 \leq x \leq L, \\ \dfrac{\mathrm{d}u}{\mathrm{d}x}(x) = i\kappa v(x) + f_v(x) & \text{for } 0 \leq x \leq L, \end{cases} \tag{49}$$

with boundary conditions at $x = 0$ et $x = L$

$$u(0) + v(0) = 0 \quad \text{et} \quad u(L) - v(L) = 0. \tag{50}$$

Using the Fredholm alternative, we can prove that the problem is well-posed for any f_u and f_v in L^2.

Problem setting 2/2

Theorem

For any $f_u \in L^2(0,L)$ *et* $f_v \in L^2(0,L)$*, there exists a unique solution* $(u,v) \in H^1(0,L) \times H^1(0,L)$.
Moreover, if $f_u \in H^q(0,L)$ *and* $f_v \in H^q(0,L)$ *then* $u \in H^{q+1}(0,L)$ *and* $v \in H^{q+1}(0,L)$.

$$\left\{ \begin{array}{lll} \|u\|_{H^{q+1}([0,L])} & \lesssim & \|f_u\|_{H^{q-1}([0,L])} + \|f_v\|_{H^q([0,L])}, \\ \|v\|_{H^{q+1}([0,L])} & \lesssim & \|f_u\|_{H^q([0,L])} + \|f_v\|_{H^{q-1}([0,L])}. \end{array} \right. \tag{51}$$

DG spaces 1/2

The domain is decomposed into N contiguous segments I_n with length δx and we have $L = N\delta x$, that is:

$$\begin{cases} x_n = n\delta x, & 0 \leq n \leq N, \\ I_n = [x_{n-1}, x_n] & 1 \leq n \leq N. \end{cases} \tag{52}$$

For any function $\varphi : [0, L] \longrightarrow \mathbb{C}$, let φ_n be the restriction of φ to I_n.

We introduce the DG spaces:

$$\begin{aligned} V &= \Big\{ u : [0, L] \longrightarrow \mathbb{C}, u \in L^2([0, L] \,\Big|\, \forall n \in [1, N] \quad u_n \in H^1(I_n) \Big\}, \\ \mathcal{V} &= \Big\{ \mathcal{V} = (u, v) \in V \times V \Big\}. \end{aligned} \tag{53}$$

Numerical trace 1/2

Definition (Numerical trace)

The numerical trace is defined by

$$\widehat{u}(0) = \frac{u_1(0) - v_1(0)}{2}, \widehat{v}(0) = \frac{v_1(0) - u_1(0)}{2}. \tag{54}$$

for $1 \leq n \leq N-1$,

$$\begin{cases} \widehat{u}(x_n) &= \dfrac{u_{n+1}(x_n) + u_n(x_n)}{2} - \dfrac{v_{n+1}(x_n) - v_n(x_n)}{2}, \\ \widehat{v}(x_n) &= \dfrac{v_{n+1}(x_n) + v_n(x_n)}{2} - \dfrac{u_{n+1}(x_n) - u_n(x_n)}{2}, \end{cases} \tag{55}$$

and

$$\widehat{u}(L) = \frac{u_N(L) + v_N(L)}{2}, \widehat{v}(L) = \frac{v_N(L) + u_N(L)}{2}. \tag{56}$$

Numerical trace 2/2

We say that the numerical trace is a generalization of the classical trace as we have:

Proposition

The exact solution $\mathcal{U} = (u, v)$ of (49) satisfies:

$$\widehat{u}(x_n) = u(x_n) \quad \text{and} \quad \widehat{v}(x_n) = v(x_n) \quad \text{for } 0 \leq n \leq N. \tag{57}$$

Proof Remark that the exact solution is continuous in the interior of the domain and that it satisfies the boundary conditions at $x = 0$ and $x = L$. □

The numerical trace is nothing but the combination between jump and mean value defined by:

$$[w]_n = w_{n+1}(x_n) - w_n(x_n) \quad \text{and} \quad \{w\}_n = \frac{w_{n+1}(x_n) + w_n(x_n)}{2}. \tag{58}$$

Plan

6 Illustration: Elastic wave propagation with HDG
- Mathematical formulation and HDG algorithm
- Illustration of gains

Plan

6 Illustration: Elastic wave propagation with HDG

- Mathematical formulation and HDG algorithm
- Illustration of gains

Elastic wave problem

New sensing devices such as fiber optic measure strain (ϵ). Therefore, we want to solve for ($\boldsymbol{u}$, $\boldsymbol{\sigma}$) to have maximum accuracy rather than replacing in terms of $\boldsymbol{u}$ only.

$$\begin{cases} -\omega^2 \boldsymbol{u} - \nabla \cdot \boldsymbol{\sigma} = \boldsymbol{f}\,, \\ \boldsymbol{\sigma} = \frac{1}{2} \boldsymbol{C} : \epsilon\,, \qquad\qquad \epsilon = \left(\nabla \boldsymbol{u} + \nabla^T \boldsymbol{u}\right), \end{cases} \tag{59}$$

The physical properties describing the medium are contained in the stiffness tensor $\boldsymbol{C}$.

Time-harmonic wave problems:

+ Easily encode the attenuation with complex-valued parameters,
+ Direct solvers allow for multiple right-hand sides once the factorization is obtained,
− Memory cost of the matrix factorization.

HDG discretization

$$\begin{cases} -\omega^2 \boldsymbol{u} - \nabla \cdot \boldsymbol{\sigma} = \boldsymbol{f}\,, \\ \boldsymbol{\sigma} = \frac{1}{2} \boldsymbol{C} : \left(\nabla \boldsymbol{u} + \nabla^T \boldsymbol{u} \right), \end{cases}$$

Hybridizable Discontinuous Galerkin method

- **Static condensation** on first-order DG Formulations **without** increasing the number of unknown: The unknown of the global matrix is **only** the numerical trace $\widehat{\boldsymbol{u}}$.
- Handle **complex geometry** (topography) with *p*-adaptivity,
- Reduces the computational cost by removing inner dofs.

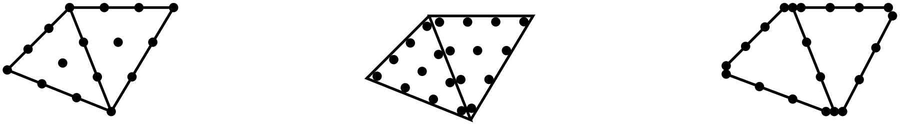

Finite Element Discontinuous Galerkin HDG

B. Cockburn J. Gopalakrishnan and R. Lazarov
Unified hybridization of discontinuous Galerkin, mixed, and continuous Galerkin methods for second order elliptic problems
SIAM Journal on Numerical Analysis (47), 2009.

HDG discretization

Hybridizable Discontinuous Galerkin method for the discretization

- Static condensation for first-order problems **without** increasing the number of unknown: The unknown of the global matrix is **only** the numerical trace $\hat{\boldsymbol{u}}$.
- Handle **complex geometry** (topography) with p-adaptivity,
- Reduces the computational cost by removing inner dofs.

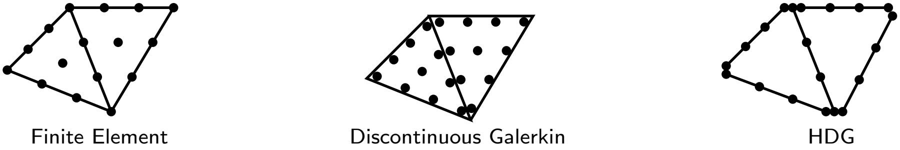

HDG is more efficient with high-order polynomial (order > 4).
High-order $\Rightarrow$ Large cell $\Rightarrow$ variable $\boldsymbol{C}$ within cells for resolution.

S.Du and F.J. Sayas
An Invitation to the Theory of the Hybridizable Discontinuous Galerkin Method: Projections, Estimates, Tools
Springer Nature, 2019

HDG Variational formulation (1/2): stiffness tensor version

The local problem is written on each cell K_e of the mesh, and the HDG problem is written in terms of $(\boldsymbol{u}, \boldsymbol{\sigma}, \widehat{u})$. Using test-functions (ψ, ϕ),

$$\begin{cases} \displaystyle\int_{K_e} -\omega^2 \boldsymbol{u}\,\overline{\psi} - \int_{K_e} \nabla\cdot\boldsymbol{\sigma}\,\overline{\psi} = \int_{K_e} \boldsymbol{f}\,\overline{\psi}, & (60a) \\ \displaystyle\int_{K_e} \frac{1}{2}\boldsymbol{C} : \nabla\boldsymbol{u}\overline{\phi} + \int_{K_e} \frac{1}{2}\boldsymbol{C} : \nabla^T\boldsymbol{u}\overline{\phi} - \int_{K_e} \boldsymbol{\sigma}\overline{\phi} = 0\,. & (60b) \end{cases}$$

To make appear the numerical trace $\widehat{u}$, we need to integrate by parts leading to derivative of $\boldsymbol{C}$.
$\Rightarrow$ **when $\boldsymbol{C}$ is not constant per cell, one would need to provide its derivative...**

Variational formulation (2/2): compliance tensor version

Using $\boldsymbol{S} = \boldsymbol{C}^{-1}$, $\begin{cases} -\omega^2 \boldsymbol{u} - \nabla \cdot \boldsymbol{\sigma} = \boldsymbol{f}\,, \\ \boldsymbol{S} : \boldsymbol{\sigma} = \frac{1}{2}\big(\nabla \boldsymbol{u} + \nabla^T \boldsymbol{u}\big)\,, \end{cases}$

On each cell K_e of the mesh,

$$\begin{cases} \displaystyle\int_{K_e} -\omega^2 \boldsymbol{u}\,\overline{\psi} - \int_{K_e} \nabla \cdot \boldsymbol{\sigma}\,\overline{\psi} = \int_{K_e} \boldsymbol{f}\,\overline{\psi}, & (61a) \\ \displaystyle\int_{K_e} \frac{1}{2}\nabla \boldsymbol{u}\overline{\phi} + \int_{K_e} \frac{1}{2}\nabla^T \boldsymbol{u}\overline{\phi} - \int_{K_e} \boldsymbol{S} : \boldsymbol{\sigma}\overline{\phi} = 0\,. & (61b) \end{cases}$$

⇒ using quadrature formula, $\boldsymbol{S}$ can easily vary within cell.

Note that under isotropy, we have an explicit formulation of $\boldsymbol{S}$ from Lamé parameters.

HDG workflow in a nutshell

Unknowns are the discretized variables: $X^h = (\boldsymbol{u}^h, \boldsymbol{\sigma}^h)$ and numerical trace $\widehat{\boldsymbol{u}}^h$.

$$\begin{cases} \text{local problem on each cell } K_e: & \mathbb{A}_e X_e^h + \mathbb{C}_e \mathcal{R}_e \widehat{\boldsymbol{u}}^h = \mathbb{F}, \\ \text{relation for numerical trace}: & \sum_e \mathcal{R}_e^T \left(\mathbb{B}_e X_e^h + \mathbb{L}_e \mathcal{R}_e \widehat{\boldsymbol{u}}^h \right) = 0. \end{cases}$$

Reorder to write **global problem** in terms of numerical trace only

$$\sum_e \mathcal{R}_e^T \left(\mathbb{L}_e - \mathbb{B}_e \mathbb{A}_e^{-1} \mathbb{C}_e \right) \mathcal{R}_e \widehat{u}_h = -\sum_e \mathcal{R}_e^T \mathbb{B}_e \mathbb{A}_e^{-1} \mathbb{F}_e \qquad \Leftrightarrow \qquad \mathcal{A}\, \widehat{\boldsymbol{u}}_h = \mathcal{B}.$$

1. Create local matrices on each cell (embarrassingly parallel) with p-adaptivity.
2. Assemble global matrix $\mathcal{A}$.
3. Solve the large linear system $\mathcal{A}\widehat{\boldsymbol{u}}^h = \mathcal{B}$ with MUMPS (solve multiple rhs at limited cost).
4. Solve the local linear systems to obtain the volume solution $(\boldsymbol{u}^h, \boldsymbol{\sigma}^h)$: (small matrices, embarrassingly parallel, $< 2\%$ of run time).

Plan

6 Illustration: Elastic wave propagation with HDG

- Mathematical formulation and HDG algorithm
- Illustration of gains

Elastic-wave propagation with HDG

3D Model with topography, size 20×20×10 km^3 with topography.

- Small cells required to accurately describe the topography, *p*-adaptivity
- Large cells elsewhere to benefit from HDG,
- models properties vary within the cell, here we use Lagrange basis per cell.

mesh

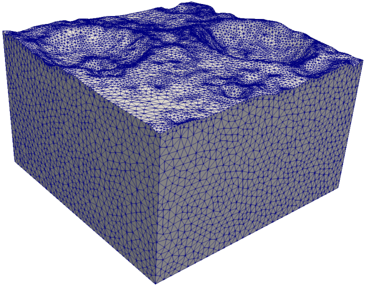

P-wave speed model.

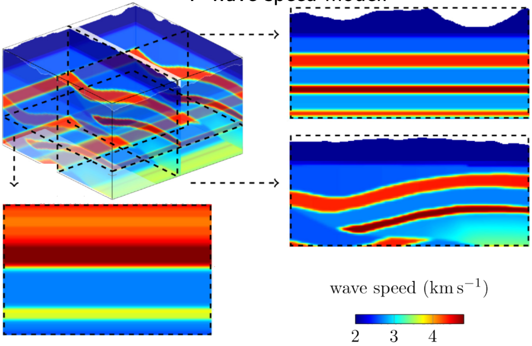

Elastic-wave propagation with HDG

3D Model with topography, size 20×20×10 km^3 with topography.

- Small cells required to accurately describe the topography, *p*-adaptivity
- Large cells elsewhere to benefit from HDG,
- models properties vary within the cell, here we use Lagrange basis per cell.

mesh

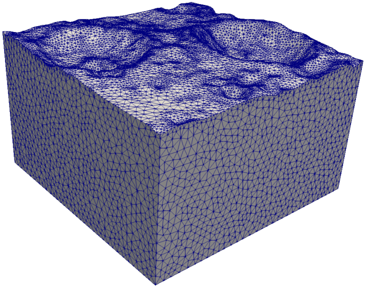

polynomial orders.

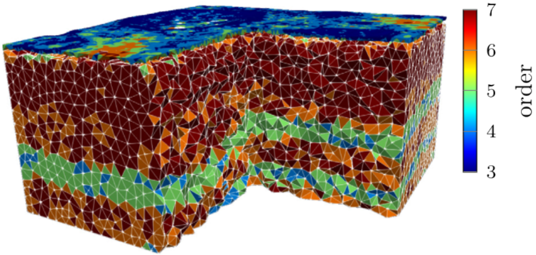

Elastic-wave propagation with HDG

3D Model with topography, size $20 \times 20 \times 10$ km^3 with topography.

- Small cells required to accurately describe the topography, *p*-adaptivity
- Large cells elsewhere to benefit from HDG,
- models properties vary within the cell, here we use Lagrange basis per cell.

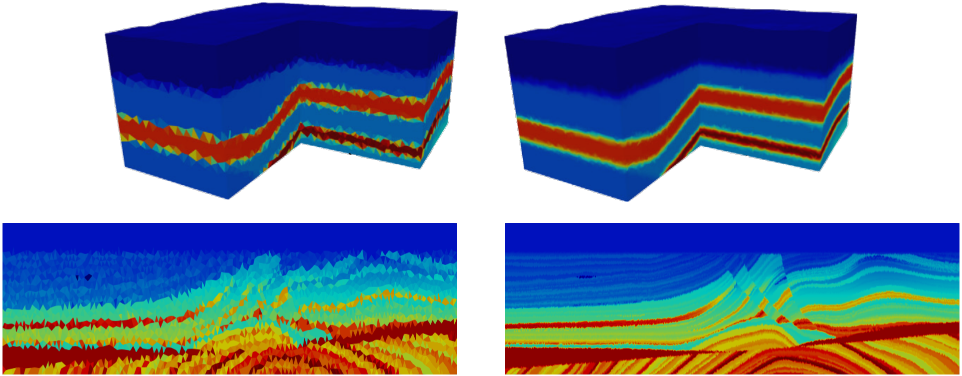

Matrix size reduction with HDG+MUMPS

3D elastic wave propagation, size 20×20×10 km^3 with topography.

Mesh using 120 000 cells

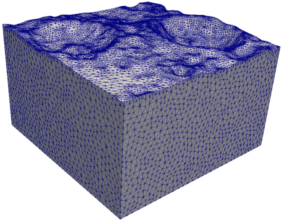

Polynomial order between 2 and 10

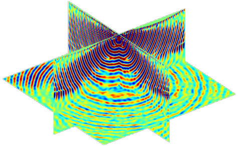

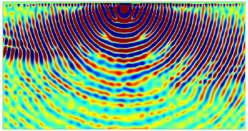

displacement field u_z at 4 Hz

Global matrix size with frequency

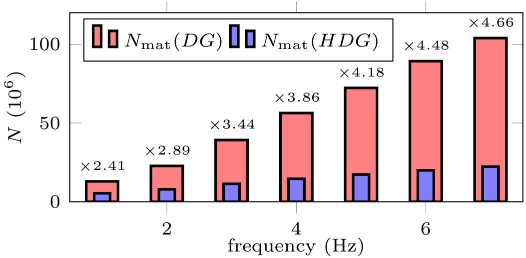

elastic simulation 7 Hz with 1600 cores **HDG+MUMPS**:

- **matrix size** $N = 22.3 \times 10^6$,
- **analysis time** 2 min 30 sec,
- **factorization time** 34 min,
- **factorization memory** 3589 GiB,
- **solve time (19 rhs)** 1 min 40 s.

Plan

7 Trefftz

Trefftz method

Erich Trefftz (1888 – 1937): 'Ein Gegenstück zum Ritzschen Verfahren' (a counterpart to Ritz' method), 1926

Principle:

- Consider local (on an element) solutions to the PDE of interest
- Construct the variational formulation locally: only element boundaries are involved
- Sum all over the elements to get a global system based upon the skeleton of the mesh.

The main advantages of the Trefftz method over the standard approach are:

- the formulation calls for integration along the element boundaries only which allows for curve-sided or polynomial shapes to be used for the element boundary
- bases for elements do not satisfy inter-element continuity through the variational functional
- this method allows for the development of crack singular or perforated elements through the use of localized solution functions as the trial functions

An anisotropic Helmholtz equation

Let A be a symetric and positive definite matrix: it represents the variation of the velocity inside the domain Ω with regular boundary $\partial\Omega$. We consider the first-order equation:

$$\begin{cases} A\nabla p(\mathbf{x}) = ik\overrightarrow{v}(\mathbf{x}) \text{ in } \Omega, \\ \text{div } \overrightarrow{v}(\mathbf{x}) = ikp(\mathbf{x}) \text{ in } \Omega, \\ Yp - \overrightarrow{v} \cdot \mathbf{n} = \varphi \text{ on } \partial\Omega, \end{cases}$$

where

- ω is the frequency
- $k = \dfrac{\omega}{c}$ is the wave number,
- $\mathbf{n}$ is the unitary normal vector supposed to be outwardly directed to $\partial\Omega$
- Y is called the admittance, it satisfies $YZ = 1$, Z being the impedance operator

The acoustic pressure p is scalar and satisfies the anisotropic Helmholtz equation. $\overrightarrow{v}$ is the velocity of the wavefield.

Discretization of the domain

- $K \in \mathcal{K}$ is an element
- ∂K is the boundary of K
- $\mathcal{K}$ is the set of the elements
- $\overline{\Omega} = \bigcup_{K \in \mathcal{K}} \overline{K}.$

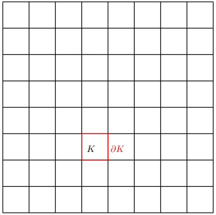

Discretization of the domain Ω.

Skeleton of the mesh

$$\partial K = \bigcup_{F \in \mathcal{F}_K} F$$

- $\mathcal{F}$ is the skeleton of the mesh
- $\mathcal{F}_K$ is the set of faces of K
- F is a face
- $\mathcal{F}_{int}$ is the set of interior faces
- $\mathcal{F}_{ext}$ is the set of exterior faces

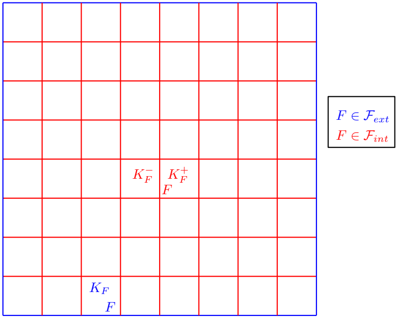

A Trefftz space for Helmholtz equation

We consider the Trefftz space defined as:

$$\mathbb{X} = \prod_{K \in \mathcal{K}} \mathbb{X}_K$$

where $(p_K, \vec{v}_K)$ is the restriction on K of $(p, \vec{v})$ and

$$\mathbb{X}_K = \Big\{ (p_K, \vec{v}_K) \in L^2(K) \times (L^2(K))^3 \ \Big| \ \operatorname{div}(\vec{v}_K) = ikp_K \text{ in } K,\ A\nabla p_K = ik\vec{v}_K \text{ in } K \text{ and } \vec{v}_K \cdot \mathbf{n}_K \in L^2(\partial K) \Big\}$$

- $\mathbb{X}_K$ contains local solutions to the Helmholtz equation
- It is a DG method: discontinuity of the basis functions between two elements

Remark

As a local solution to Helmholtz equation, p_K is $H^1(K)$ and $\vec{v}_K$ is $H(div, K)$

Virtual work principle

Assume that the continuous problem admits a regular solution $(p, \overrightarrow{v})$. Let $(p', \overrightarrow{v}')$ be in $\mathbb{X}$. Then if restricted to an element K, it is solution to the problem of interest. Hence, we have:

$$\int_K \nabla p \cdot \overrightarrow{v}'_K + \text{div } \overrightarrow{v} \; p' = W_K$$

where W_K is defined by:

$$W_K = ik \int_K A^{-1}\overrightarrow{v} \cdot \overrightarrow{v}' + p \, p'$$

Since $(p', \overrightarrow{v}')$ is in $\mathbb{X}$, integrating by parts, we obtain that:

Proposition

Let $(p, \overrightarrow{v})$ be a solution to the continuous problem. Then for any $(p', \overrightarrow{v}')$ in $\mathbb{X}$,

$$W_K = \frac{1}{2} \int_{\partial K} p \, \overline{\overrightarrow{v}'} \cdot \mathbf{n} + p' \, \overline{\overrightarrow{v}} \cdot \mathbf{n}$$

Virtual work principle

Then, applying the virtual work principle, we have:

$$\sum_{K\in\mathcal{K}} W_K = 0$$

which is equivalent to:

$$\sum_{K\in\mathcal{K}} \int_{\partial K} \vec{v}_K \cdot \mathbf{n}_K \, \overline{p'_K} + p_K \, \overline{\vec{v}'_K \cdot \mathbf{n}_K} \; = \; 0,$$

We then rewrite this expression in terms of jumps to end up with a variational formulation set on the skeleton of the mesh:

Variational formulation

$$\sum_{F\in\mathcal{F}_{int}} \int_F \overrightarrow{v}_F\, \overline{[\![p']\!]_F} + p_F\, \overline{[\![\overrightarrow{v}']\!]_F} + \sum_{F\in\mathcal{F}_{ext}} \int_F \overrightarrow{v}_F\, \overline{p'_{K_F}}\mathbf{n}_F + p_F\, \overline{\overrightarrow{v}'_{K_F}}\cdot\mathbf{n}_F \;=\; 0,$$

where

- p_F and $\overrightarrow{v}_F$ are the traces of p and $\overrightarrow{v}$ on F,
- $\mathbf{n}_F$ is the unitary outgoing normal to the face F.

Jumps are defined by

$$[\![\overrightarrow{v}]\!]_F = \overrightarrow{v}_{K_F^+}\cdot\mathbf{n}_{K_F^+} + \overrightarrow{v}_{K_F^-}\cdot\mathbf{n}_{K_F^-}, \quad [\![p]\!]_F = p_{K_F^+}\mathbf{n}_{K_F^+} + p_{K_F^-}\mathbf{n}_{K_F^-},$$

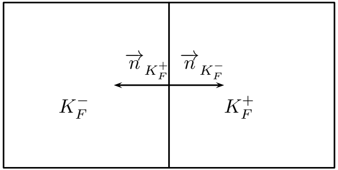

The upwind flux methods

The unknowns are the traces $\vec{v}_F$ and p_F of the unknowns $\vec{v}$ and p satisfying:

$$\sum_{F\in\mathcal{F}_{int}} \int_F \vec{v}_F\,\overline{[\![p']\!]_F} + p_F\,\overline{[\![\vec{v}\,']\!]_F} + \sum_{F\in\mathcal{F}_{ext}} \int_F \vec{v}_F\,\overline{p'_{K_F}}\mathbf{n}_F + p_F\,\overline{\vec{v}\,'_{K_F}}\cdot\mathbf{n}_F \;=\; 0,$$

We introduce outgoing and incoming fluxes:

$$\begin{aligned}\text{incoming}: \quad \gamma^- &= Y_K p_K - \vec{v}_K\cdot\mathbf{n}_K,\\ \text{outgoing}: \quad \gamma^+ &= Y_K p_K + \vec{v}_K\cdot\mathbf{n}_K.\end{aligned}$$

Remark that we have:

$$2Y_K p_K = \gamma^- + \gamma^+,\; 2\vec{v}_K\cdot\mathbf{n}_K = \gamma^+_K - \gamma^-_K$$

We seek now for generalized traces which are built by exploiting the property that as far as the exact solution is concerned, p and $\vec{v}\cdot\mathbf{n}$ are continuous across F.

The upwind flux methods

Regarding the trace of p, imposing that $p_K = p_T = p_F$, we obtain that necessarily

$$p_F = \tfrac{1}{Y_T+Y_K}\left(Y_K p_K + \overrightarrow{v}_K \cdot \mathbf{n}_K\right) + \tfrac{1}{Y_T+Y_K}\left(Y_T p_T + \overrightarrow{v}_T \cdot \mathbf{n}_T\right).$$

We thus use the generalized trace

$$\widehat{p_F} = \frac{Y_T p_T + Y_K p_K}{Y_T + Y_K} + \frac{1}{Y_T + Y_K} [\![\overrightarrow{v}]\!]_F,$$

We do the same for $\widehat{\overrightarrow{v}}_F$ and for boundary faces.
For Y_T, we use the admittance of the infinite medium :

$$Y_T = \frac{1}{(\mathbf{n} \cdot \mathbf{A}^T \mathbf{n})^{\frac{1}{2}}}$$

Anisotropic acoustic plane waves, See Ibrahima Djiba poster!

Plane waves $\mathcal{U}_{\mathrm{d}} = (p_{\vec{d}}, \vec{v}_{\vec{d}})$

$$\begin{cases} p_{\vec{d}}(\vec{x}) &= p_0 \exp\left(ik\,\vec{d}\cdot\vec{x}\right), \\ \vec{v}_{\vec{d}}(\mathrm{x}) &= \mathbf{A}\,\vec{d}\,p_0 \exp\left(ik\,\vec{d}\cdot\vec{x}\right). \end{cases}$$

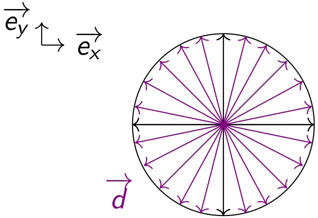

- $\vec{d}$ the direction of the plane wave
- $k = \frac{\omega}{c}$ the wave number

The discrete Trefftz space is spanned by

$$\mathcal{U}_{K,n}(\vec{x}) = 0 \text{ if } \vec{x} \notin K$$

$$\mathcal{U}_{K,n}(\vec{x}) = \mathcal{U}_{(\cos(n\delta\theta),\sin(n\delta\theta))}(\vec{x}) \text{ if } \vec{x} \in K \text{ with } \delta\theta = \frac{2\pi}{N}.$$

Discussion

- Numerics show that it is not efficient to increase the number of plane waves
- Numerics show that is not relevant to decrease the discretization step too much
- It is difficult to construct Trefftz spaces: consider quasi-Trefftz functions resulting from another code (BEM, CG)
- Conditioning is key

Some references on Trefftz implementation

What is the optimal number of plane waves?

- Moiola, A. (2011). Trefftz-discontinuous Galerkin methods for time-harmonic wave problems (Doctoral dissertation, ETH Zurich). (Page 156).
- Moiola, A., Hiptmair, R., Perugia, I. (2011). Vekua theory for the Helmholtz operator. Zeitschrift für angewandte Mathematik und Physik, 62(5), 779-807.

Basis reduction → improvement in conditioning

- T. Luostari, T. Huttunen, P. Monk, (2013). Improvements for the ultra weak variational formulation, Int. J. Numer. Meth. Engng 94, 598624.
- S. Congreve, J. Gedicke, I. Perugia, (2019). Numerical investigation of the conditioning for plane wave discontinuous Galerkin methods, Vol. 126 of Lecture Notes in Computational Science and Engineering, Springer.
- H. Barucq, A. Bendali, J. Diaz, S. Tordeux, (2021). Local strategies for improving the conditioning of the plane-wave Ultra-Weak Variational Formulation. Journal of Computational Physics, 441, 110449.

Some references on Trefftz implementation

Alternatives to plane waves exist

- Evanescent modes
  - E. Parolin, D. Huybrechs, A. MOIOLA, (2022). Stable approximation of Helmholtz solutions by evanescent plane waves. arXiv preprint 2202.05658.
- Quasi-Trefftz methods
  - LM. Imbert-Gerard, G. Sylvand, Three types of quasi-Trefftz functions for the 3D convected Helmholtz equation: construction and approximation properties, preprint
  - H. S. Fure, S. Pernet, M. Sirdey, S. Tordeux, (2020). A discontinuous Galerkin Trefftz type method for solving the two dimensional Maxwell equations. SN Partial Differ. Equ. Appl. 1, 23.

Plan

8 Inverse problem
- Iterative minimization algorithm
- Numerical experiment

Plan

8 Inverse problem
- Iterative minimization algorithm
- Numerical experiment

Quantitative reconstruction algorithm: FWI

Quantitative reconstruction of properties $\boldsymbol{m} = (\lambda, \mu, \rho)$ solving iterative minimization problem.

$$\min_{\boldsymbol{m}} \mathcal{J}(\boldsymbol{m}) \quad \text{with} \quad \mathcal{J}(\boldsymbol{m}) = \mathrm{dist}\big(\mathcal{F}(\boldsymbol{m}), \boldsymbol{d}\big), \quad \mathcal{F}\text{: simulations}, \quad \boldsymbol{d}\text{: observations}.$$

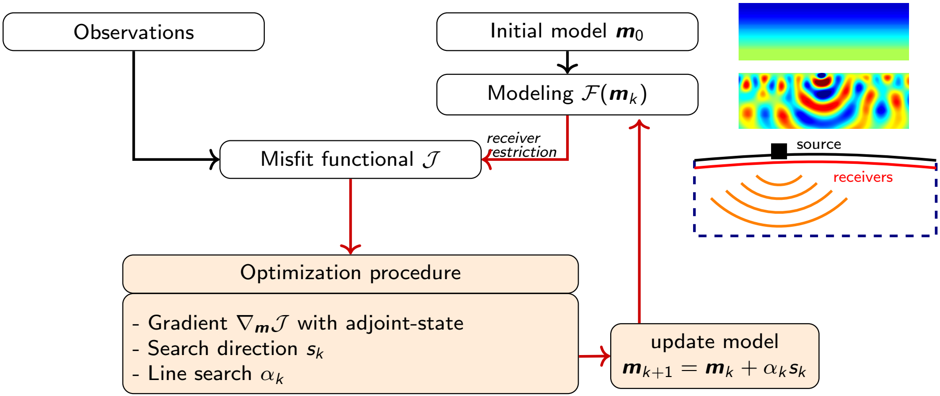

Quantitative reconstruction algorithm: FWI

minimize $\mathcal{J}(\boldsymbol{m}) = \mathrm{dist}\big(\mathcal{F}(\boldsymbol{m}),\, \boldsymbol{d}\,\big)$

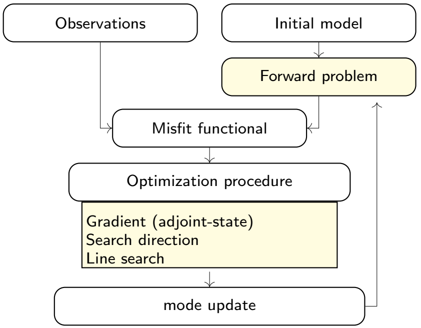

1. Repeated use of forward wave propagation solver,

$$\begin{cases} \mathbb{A}_e X_e^h + \mathbb{C}_e \mathcal{R}_e \widehat{\boldsymbol{u}}^h = \mathbb{F}\,, & (62a) \\ \sum_e \mathcal{R}_e^T \left(\mathbb{B}_e X_e^h + \mathbb{L}_e \mathcal{R}_e \widehat{\boldsymbol{u}}^h \right) = 0\,. & (62b) \end{cases}$$

2. Adjoint-state method for gradient adapted to HDG Lagrangian written from $\mathcal{J}$ subject to (62a), (62b).

We prove that for HDG, the gradient is still computed from the **adjoint of the direct problem**, fundamental to avoid refactorization of the global matrix.

Quantitative reconstruction algorithm: FWI

minimize $\quad \mathcal{J}(\boldsymbol{m}) = \mathrm{dist}\big(\mathcal{F}(\boldsymbol{m}), \boldsymbol{d}\,\big)$

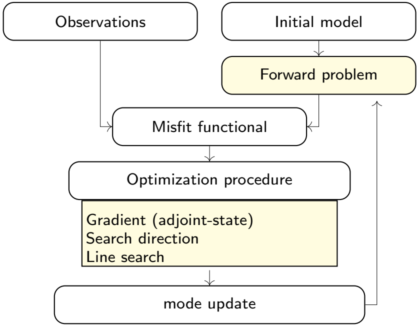

1. Repeated use of forward wave propagation solver,
2. Adjoint-state method for gradient adapted to HDG,
3. To alleviate mesh limitations, the model parameters are represented with Lagrange basis functions.
4. Inversion is carried out with respect to the weight of the Lagrange basis functions.

Plan

8. Inverse problem
   - Iterative minimization algorithm
   - Numerical experiment

2D experiments: Marmousi II setup

We consider the elastic isotropic Marmousi II experiment, of size 17×3.5 km^2.
Free-surface boundary condition on top and absorbing boundary conditions elsewhere.

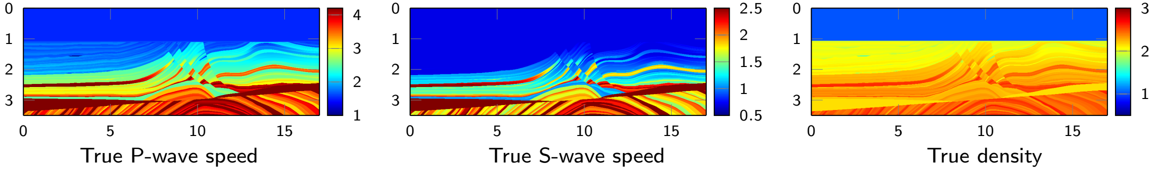

2D experiments: Marmousi II setup

We consider the elastic isotropic Marmousi II experiment, of size 17×3.5 km^2.
Free-surface boundary condition on top and absorbing boundary conditions elsewhere.

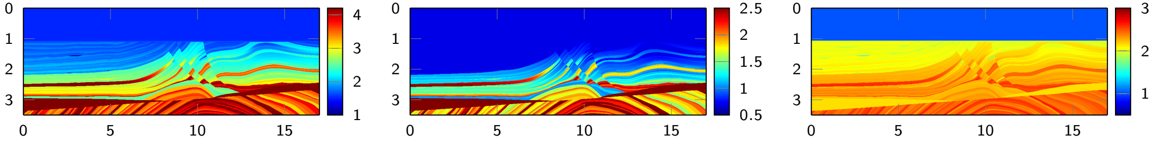

True P-wave speed | True S-wave speed | True density

Initial models are 1D-background variation.

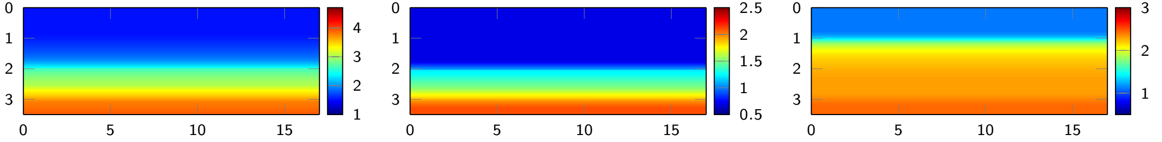

Initial P-wave speed | Initial S-wave speed | Initial density

2D experiments: Marmousi II reconstructions

- Acquisition made up of 169 sources and 849 receivers near surface.
- Reconstructions using 13 frequencies from 2 to 8 Hz, 25 iterations per frequency.
- Density is not inverted and remains in its initial value.

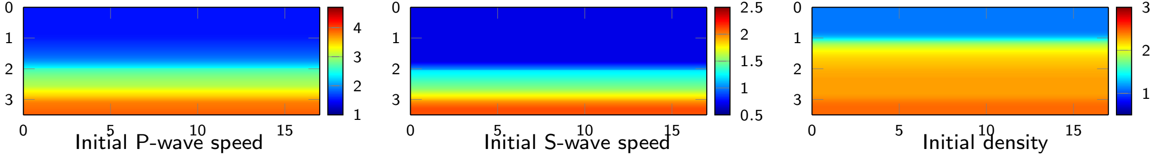

2D experiments: Marmousi II reconstructions

- Acquisition made up of 169 sources and 849 receivers near surface.
- Reconstructions using 13 frequencies from 2 to 8 Hz, 25 iterations per frequency.
- Density is not inverted and remains in its initial value.

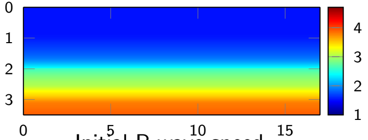

Initial P-wave speed

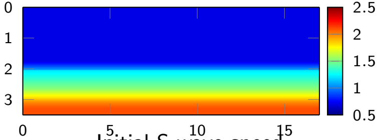

Initial S-wave speed

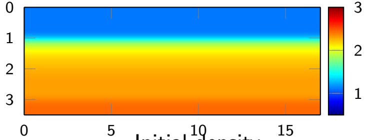

Initial density

- Reconstruction using representation in order 1 Lagrange basis per cell ($\sim 20 \times 10^3$ cells)

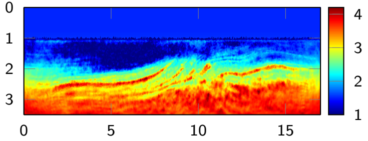

Reconstruction P-wave speed

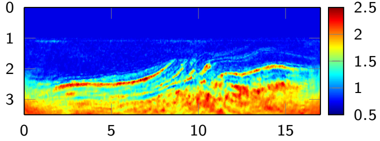

Reconstruction S-wave speed

2D experiments: Marmousi II reconstructions

- Acquisition made up of 169 sources and 849 receivers near surface.
- Reconstructions using 13 frequencies from 2 to 8 Hz, 25 iterations per frequency.
- Density is not inverted and remains in its initial value.

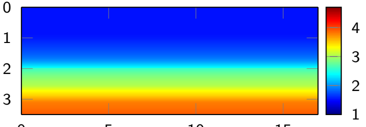

Initial P-wave speed

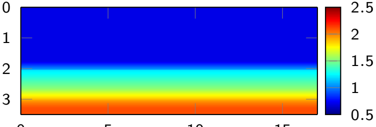

Initial S-wave speed

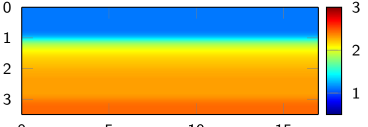

Initial density

- Computational time (`18mpi` $\times$ `2omp`): $2{\cdot}10^4$ cells: 3h; $5{\cdot}10^4$ cells: 4h15min, i.e. **-30%**.

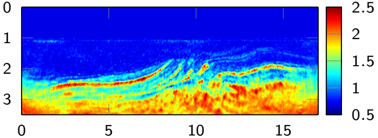

S-wave speed reconstruction using mesh with 20 000 cells and Lagrange basis representation,

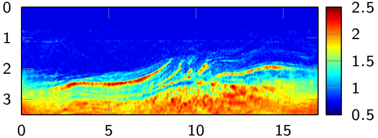

S-wave speed reconstruction using mesh with 50 000 cells piecewise-constant representation.

Plan

9. Helioseismology/asteroseismology
   - Modal Green's kernel
   - Numerical experiments
   - Power spectrum, comparison with measured data
   - The vector wave problem

Helioseismic studies

- Measuring solar/star oscillations,
- Processing and averaging the observations to extract the seismic data
- Interpreting the seismic data using forward and inverse methods to estimate solar internal properties.

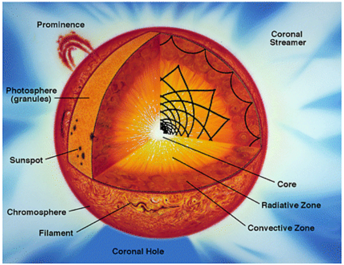

Solar interior

Detecting active regions on the far side of the Sun

- Of great importance for space-weather forecasts
- Large active regions that emerge on the Sun's far side will rotate into Earth's view several days later; these may trigger coronal mass ejections, which can damage satellites and spacecraft and endanger astronauts
- It is known that far-side imaging can significantly improve models of the solar wind, which plays an important role in space-weather forecasts.

.

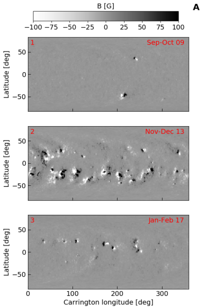

Numerical simulations of acoustic waves, see Lola Chabat Poster!

Acoustic waves propagate horizontally and are trapped in the vertical direction; they connect the Sun's near and far sides. As acoustic waves travel faster in magnetized regions, they can inform us about the presence of active regions along their paths of propagation.

Two helioseismic techniques:

- Helioseismic holography: multiply the forward and backward propagated wavefields,and subtract a reference measurement for the quiet Sun.
- Time-distance helioseismology: compute the cross-covariance of the wavefield

Develop models and computational tools that are required to recover information about Sun and eventually stellar activity from observations of oscillations.

C. Lindsey and D.C. Braun, Helioseismic holography. The Astrophysical Journal, 1997

L. Gizon,H. Barucq, M. Duruflé, C.S. Hanson, M. Leguèbe, A.C. Birch, J. Chabassier, D. Fournier, T. Hohage and E. Papini, Computational helioseismology in the frequency domain: acoustic waves in axisymmetric solar models with flows. Astronomy & Astrophysics, 2017

Equations

- **Galbrun's equation** describes adiabatic wave motion subject to source F with frequency ω, on top of a time-invariant fluid background. Ignoring flows and rotation and with Cowling's approximation,

$$-\rho_0(\omega^2+2\,\mathrm{i}\omega\,\Gamma)\,\xi-\nabla\left[\gamma\,p_0\nabla\cdot\xi\right]+(\nabla\,p_0)(\nabla\cdot\xi)-\nabla\,(\xi\cdot\nabla\,p_0)+(\xi\cdot\nabla)\nabla\,p_0+\rho_0\,(\xi\cdot\nabla)\nabla\,\phi_0\;=\;F\,,$$

with displacement vector ξ describing the solar oscillation. The density is ρ_0, pressure p_0, adiabatic index γ, gravitational potential ϕ_0 and attenuation Γ.

H. Barucq, F. Faucher, D. Fournier, L. Gizon and H. Pham, Efficient and accurate algorithm for the full modal Green's kernel of the scalar wave equation in helioseismology. SIAM J. on Appl. Math., 2020.

H. Barucq, F. Faucher, D. Fournier, L. Gizon and H. Pham, Outgoing modal solutions for Galbrun's equation in helioseismology. J. of Differential Eq., 2021.

Equations

- **Galbrun's equation** describes adiabatic wave motion subject to source F with frequency ω, on top of a time-invariant fluid background. Ignoring flows and rotation and with Cowling's approximation,

$$-\rho_0(\omega^2+2\,\mathrm{i}\omega\,\Gamma)\,\xi-\nabla\left[\gamma\,p_0\nabla\cdot\xi\right]+(\nabla\,p_0)(\nabla\cdot\xi)-\nabla\,(\xi\cdot\nabla\,p_0)+(\xi\cdot\nabla)\nabla\,p_0+\rho_0\,(\xi\cdot\nabla)\nabla\,\phi_0 \;=\; F\,,$$

  with displacement vector ξ describing the solar oscillation. The density is ρ_0, pressure p_0, adiabatic index γ, gravitational potential ϕ_0 and attenuation Γ.

- Further approximation ignoring the gravity, we obtain a **scalar-wave equation** for variable $u := \rho\,c^2\nabla\cdot\xi$ such that,

$$-\nabla\cdot\left(\frac{1}{\rho}\nabla u\right)-\frac{\omega^2+2\,\mathrm{i}\omega\,\Gamma}{\rho\,c^2}u = f\,, \qquad \text{with sound-speed } c.$$

H. Barucq, F. Faucher, D. Fournier, L. Gizon and H. Pham, Efficient and accurate algorithm for the full modal Green's kernel of the scalar wave equation in helioseismology. SIAM J. on Appl. Math., 2020.

H. Barucq, F. Faucher, D. Fournier, L. Gizon and H. Pham, Outgoing modal solutions for Galbrun's equation in helioseismology. J. of Differential Eq., 2021.

Spherical background solar model

Model S+Atmo: exponentially decreasing density in the solar atmosphere

$$\rho(r) := \begin{cases} \rho_S(r)\,, & r \leq r_a \\ \rho_S(r_a)\; e^{-\alpha_\infty\,(r-r_a)}\,, & r > r_a \end{cases}, \qquad c(r) := \begin{cases} c_S(r), & r \leq r_a; \\ c_S(r_a), & r > r_a \end{cases}$$

with $\rho_S > \rho_0 > 0$; $c_S > c_0 > 0$, $R_\odot =$ the solar radius ($\sim 696 \times 10^3$km)

Spherical background solar model

Model S+Atmo: exponentially decreasing density in the solar atmosphere

$$\rho(r) := \begin{cases} \rho_S(r)\,, & r \leq r_a \\ \rho_S(r_a)\; e^{-\alpha_\infty\,(r - r_a)}\,, & r > r_a \end{cases}, \qquad c(r) := \begin{cases} c_S(r), & r \leq r_a; \\ c_S(r_a), & r > r_a \end{cases}$$

Comparison of the S+Atmo (solid) and VAL-C (dashed) atmospheric models.

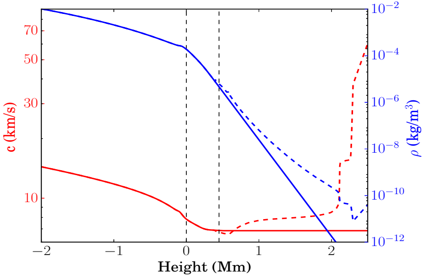

Height above surface (Mm) R_h	0.5	0.556	2.543	4
scaled radius $= (R_\odot + R_h)/R_\odot$	1.0007	1.0008	1.0037	1.0058

Scalar-wave problem formulation, spherical symmetry

$$-\nabla \cdot \left(\frac{1}{\rho} \nabla u \right) - \frac{\omega^2 + 2\,\mathrm{i}\omega\,\Gamma}{\rho\, c^2} u = f\,.$$

H. Barucq, F. Faucher, D. Fournier, L. Gizon and H. Pham, Efficient and accurate algorithm for the full modal Green's kernel of the scalar wave equation in helioseismology. SIAM J. on Appl. Math., 2020.

H. Barucq, F. Faucher, H. Pham, Outgoing solutions and radiation boundary conditions for the ideal atmospheric scalar wave equation in helioseismology. ESAIM, 2020.

Scalar-wave problem formulation, spherical symmetry

$$-\nabla\cdot\left(\frac{1}{\rho}\nabla \mathfrak{u}\right) - \frac{\omega^2 + 2\,\mathrm{i}\omega\,\Gamma}{\rho\, c^2}\mathfrak{u} = \mathfrak{f}\,.$$

1. We use the Liouville transform to rewrite the problem in Schrödinger form,

With $u = \rho^{-1/2}\mathfrak{u}$ and $\alpha = -\rho'/\rho$, we obtain

$$\left(-\Delta - \frac{\omega^2 + 2\,\mathrm{i}\omega\,\Gamma}{c^2} + \frac{\alpha^2}{4} + \frac{\alpha'}{2} + \frac{\alpha}{r}\right) u = f\,.$$

In the atmosphere, ρ is exponentially decreasing $\Rightarrow$ α is constant.

H. Barucq, F. Faucher, D. Fournier, L. Gizon and H. Pham, Efficient and accurate algorithm for the full modal Green's kernel of the scalar wave equation in helioseismology. SIAM J. on Appl. Math., 2020.

H. Barucq, F. Faucher, H. Pham, Outgoing solutions and radiation boundary conditions for the ideal atmospheric scalar wave equation in helioseismology. ESAIM, 2020.

Scalar-wave problem formulation, spherical symmetry

$$-\nabla \cdot \left(\frac{1}{\rho} \nabla \mathfrak{u} \right) - \frac{\omega^2 + 2\,\mathrm{i}\omega\,\Gamma}{\rho\, c^2} \mathfrak{u} = \mathfrak{f}\,.$$

1. We use the Liouville transform to rewrite the problem in Schrödinger form,

With $u = \rho^{-1/2}\mathfrak{u}$ and $\alpha = -\rho'/\rho$, we obtain

$$\left(-\Delta - \frac{\omega^2 + 2\,\mathrm{i}\omega\,\Gamma}{c^2} + \frac{\alpha^2}{4} + \frac{\alpha'}{2} + \frac{\alpha}{r} \right) u = f\,,$$

In the atmosphere, ρ is exponentially decreasing $\Rightarrow$ α is constant.

2. Allows us to build the exact Dirichlet-to-Neumann map and new classes of Radiation Boundary conditions for outgoing solutions.

H. Barucq, F. Faucher, D. Fournier, L. Gizon and H. Pham, Efficient and accurate algorithm for the full modal Green's kernel of the scalar wave equation in helioseismology. SIAM J. on Appl. Math., 2020.

H. Barucq, F. Faucher, H. Pham, Outgoing solutions and radiation boundary conditions for the ideal atmospheric scalar wave equation in helioseismology. ESAIM, 2020.

Cross-covariance in terms of Green's function

At frequency ω, consider the cross-covariance in Fourier space as the product of the wave field at two locations of measurement,

$$C(r_1, r_2, \omega) = \Psi^*(r_1, \omega)\Psi(r_2, \omega)$$

Here, $\Psi = c\nabla \cdot \xi$. In terms of the Green's function, we have

$$\Psi(r_j, \omega) = \int_V G(r_j, r, \omega) s(r, \omega) \rho dr$$

where the source $s(r, \omega)$ is a realization of a random process.

Plan

9. Helioseismology/asteroseismology
    - Modal Green's kernel
    - Numerical experiments
    - Power spectrum, comparison with measured data
    - The vector wave problem

Modal Green's kernel

Decomposition on harmonic mode ℓ, the modal Green's kernel G_ℓ solves,

$$\mathcal{L}\, G_\ell(r,s) = \delta(r-s), \qquad \text{with} \quad \mathcal{L} := \left(-\partial_r^2 - \frac{\omega^2 + 2\,\mathrm{i}\omega\,\Gamma}{c^2} + \frac{\alpha^2}{4} + \frac{\alpha'}{2} + \frac{\alpha}{r} + \frac{\ell(\ell+1)}{r^2} \right).$$

with Neumann boundary condition at origin: $\partial_n G_\ell(r=0) = 0,$

and radiation condition at $r = r_{\max}$: $(\partial_n G_\ell \,-\, \mathcal{Z}\, G_\ell)_{r=r_{\max}} = 0.$

H. Barucq, F. Faucher, H. Pham, Outgoing solutions and radiation boundary conditions for the ideal atmospheric scalar wave equation in helioseismology. ESAIM, 2020.

Modal Green's kernel

Decomposition on harmonic mode ℓ, the modal Green's kernel G_ℓ solves,

$$\mathcal{L}\, G_\ell(r,s) = \delta(r-s), \qquad \text{with} \quad \mathcal{L} := \left(-\partial_r^2 - \frac{\omega^2 + 2\,\mathrm{i}\omega\,\Gamma}{c^2} + \frac{\alpha^2}{4} + \frac{\alpha'}{2} + \frac{\alpha}{r} + \frac{\ell(\ell+1)}{r^2} \right).$$

with Neumann boundary condition at origin: $\partial_n G_\ell(r=0) = 0,$
and radiation condition at $r = r_{\text{max}}$: $(\partial_n G_\ell \; - \; \mathcal{Z}\, G_\ell)_{r=r_{\text{max}}} = 0.$

Computation of the modal Green's kernel:

- **Approach 1 (naive)**: for each source position s, solving equation $\mathcal{L}\, G_\ell(r,s) = \delta(r-s)$ gives $G_\ell(\cdot, s)$.

- **Approach 2**: Use an assembling formula, the entire kernel is obtained from the solutions of only two boundary-value problems.

H. Barucq, F. Faucher, D. Fournier, L. Gizon and H. Pham, Efficient and accurate algorithm for the full modal Green's kernel of the scalar wave equation in helioseismology. SIAM J. on Appl. Math., 2020.

Computation of the Green's kernel: Approach 2

- **Approach 1 (naive)**: for each source position s, solve equation $\mathcal{L}\, G_\ell(r,s) = \delta(r-s)$.
- **Approach 2**: Use an assembling formula, the entire kernel is obtained from the solutions of only two boundary-value problems.

1. Find ψ_1 that solves
$$\begin{cases} \mathcal{L}\,\psi_1 = 0\,, \quad \text{on } (0, r_{\max}), \\ (\partial_n \psi_1)_{r=0} = 0, \qquad (\psi_1)_{r=r_b} = 1\,. \end{cases}$$

2. Find ψ_2 that solves
$$\begin{cases} \mathcal{L}\,\psi_2 = 0\,, \quad \text{on } (r_a, r_{\max}), \\ (\psi_2)_{r=r_a} = 1, \qquad (\partial_n \psi_2 - \mathcal{Z}\psi_2)_{r=r_{\max}} = 0\,. \end{cases}$$

H. Barucq, F. Faucher, D. Fournier, L. Gizon and H. Pham, Efficient and accurate algorithm for the full modal Green's kernel of the scalar wave equation in helioseismology. SIAM J. on Appl. Math., 2020.

Computation of the Green's kernel: Approach 2

- **Approach 1 (naive)**: for each source position s, solve equation $\mathcal{L}\, G_\ell(r,s) = \delta(r-s)$.
- **Approach 2**: Use an assembling formula, the entire kernel is obtained from the solutions of only two boundary-value problems.

1. Find ψ_1 that solves
$$\begin{cases} \mathcal{L}\,\psi_1 = 0\,, & \text{on } (0, r_{\max}), \\ (\partial_n \psi_1)_{r=0} = 0, & (\psi_1)_{r=r_b} = 1\,. \end{cases}$$
2. Find ψ_2 that solves
$$\begin{cases} \mathcal{L}\,\psi_2 = 0\,, & \text{on } (r_a, r_{\max}), \\ (\psi_2)_{r=r_a} = 1, & (\partial_n \psi_2 - \mathcal{Z}\psi_2)_{r=r_{\max}} = 0\,. \end{cases}$$
3. Assemble the Green's kernel, with H the Heaviside and $\mathcal{W}$ the Wronskian $\mathcal{W}(s) := \mathcal{W}\{\psi_1(s), \psi_2(s)\}$,

$$G_\ell(r,s) = \frac{-H(s-r)\,\psi_1(r)\,\psi_2(s) - H(r-s)\,\psi_1(s)\,\psi_2(r)}{\mathcal{W}(s)}, \qquad \forall\,(r,s) \in (r_a, r_{\max}),$$

H. Barucq, F. Faucher, D. Fournier, L. Gizon and H. Pham, Efficient and accurate algorithm for the full modal Green's kernel of the scalar wave equation in helioseismology. SIAM J. on Appl. Math., 2020.

Computation of the Green's kernel: Approach 2

- **Approach 1 (naive)**: for each source position s, solve equation $\mathcal{L}\, G_\ell(r,s) = \delta(r-s)$.
- **Approach 2**: Use an assembling formula, the entire kernel is obtained from the solutions of only two boundary-value problems.

Approach 1: the solution of one problem for a Dirac in s_0 only gives $G_\ell(r, s = s_0)$ and $G_\ell(r = s_0, s)$.

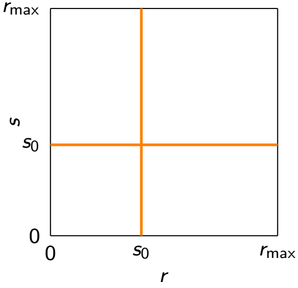

Approach 2: from the solutions of two boundary value problems, $G_\ell(r,s)$ is obtained for any position between r_a and r_b.

It also avoids the singularity of the Dirac source.

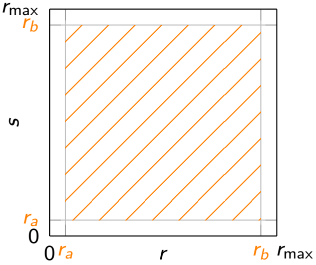

Plan

9. Helioseismology/asteroseismology
   - Modal Green's kernel
   - Numerical experiments
   - Power spectrum, comparison with measured data
   - The vector wave problem

Solar Green's kernels

- The background sound-speed and density are given by `model S+Atmo` or model `Val-C`.

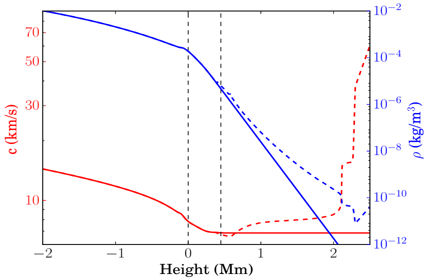

Solar Green's kernels

- The background sound-speed and density are given by `model S+Atmo` or model `Val-C`.
- The Green's kernel is computed with Approach 2 which only need the solutions of two problems.

Imaginary part of the Solar modal Green's functions at 7 mHz for mode $\ell = 100$ using different background.

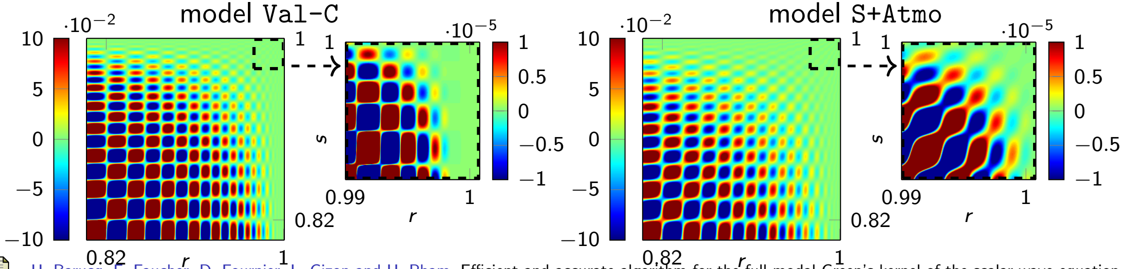

H. Barucq, F. Faucher, D. Fournier, L. Gizon and H. Pham, Efficient and accurate algorithm for the full modal Green's kernel of the scalar wave equation in helioseismology. SIAM J. on Appl. Math., 2020

F. Faucher
hawen: time-harmonic wave modeling and inversion using hybridizable discontinuous Galerkin discretization
Journal of Open Source Software, 6 (57), 2021

Solar Green's kernels

- The background sound-speed and density are given by `model S+Atmo` or model `Val-C`.
- The Green's kernel is computed with Approach 2 which only needs the solutions of two problems.

Approach 2 is more **efficient** as it only needs two boundary value problems to assemble the entire kernel, and more **accurate** as it avoids the Dirac singularity.

1. To obtain $G_\ell(s, s)$ with Approach 1, we need 4000 simulations,
2. Approach 1 needs a refined discretization mesh to capture correctly the singularity.

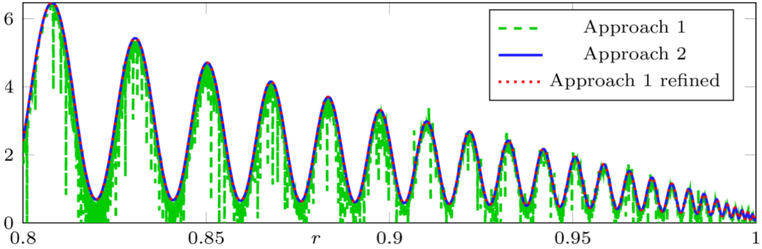

Plan

9 Helioseismology/asteroseismology

- Modal Green's kernel
- Numerical experiments
- Power spectrum, comparison with measured data
- The vector wave problem

Power spectrum

Observables are an average over height of G_ℓ, in first approximation (depending on the assumption on the source), one can consider the Power Spectrum to be directly related to the Imaginary part of G_ℓ,

$$\mathcal{P}_\ell(\omega) \propto \Big| \mathrm{Im}\big(G_\ell(\omega)(r_0, s_0)\big) \Big|^2 . \tag{67}$$

We can compare the numerical power spectrum, i.e., using Green's function computed for harmonic degrees (modes) ℓ and frequencies $\omega/(2\pi)$, with observations.

H. Barucq, F. Faucher, D. Fournier, L. Gizon and H. Pham, Efficient and accurate algorithm for the full modal Green's kernel of the scalar wave equation in helioseismology. SIAM J. on Appl. Math., 2020.

Power spectrum

We evaluate the imaginary part of the Green's function $G_\ell(r = 1, s = 1)$ with frequencies and modes, using `model S+Atmo`.

$$\ell \in (0,\ 1000), \qquad \omega/(2\pi) \in (0, 10)\text{mHz}.$$

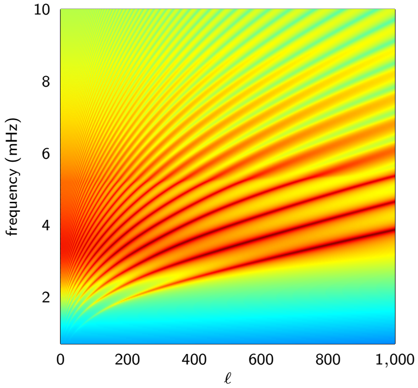

Power spectrum

We evaluate the imaginary part of the Green's function $G_\ell(r=1, s=1)$ with frequencies and modes, using `model S+Atmo`.

Comparison with HMI data (white crosses), for $\ell \in (0,\, 100)$, $\omega/(2\pi) \in (0.5,\, 4)$mHz.

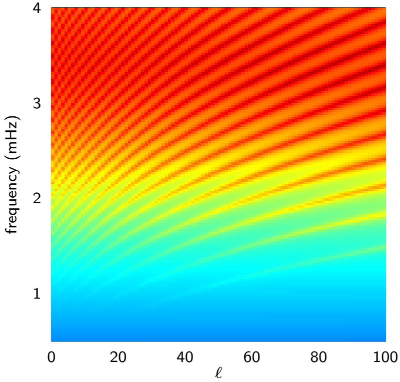

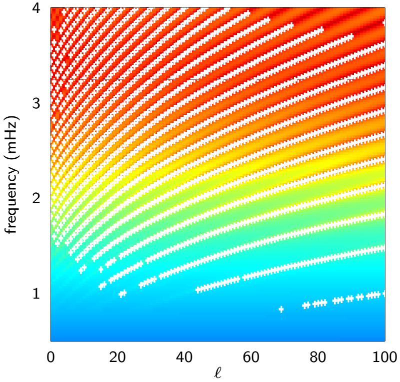

Plan

9. Helioseismology/asteroseismology
    - Modal Green's kernel
    - Numerical experiments
    - Power spectrum, comparison with measured data
    - The vector wave problem

Vector-wave equation with gravity

The same method can be applied to the vector-wave problem (Vector Spherical Harmonics),

$$-\rho_0\left(\omega^2+2\,\mathrm{i}\omega\,\Gamma\right)\,\xi-\nabla\left[\gamma\,p_0\nabla\cdot\xi\right]+(\nabla\,p_0)(\nabla\cdot\xi)-\nabla\,(\xi\cdot\nabla\,p_0)+(\xi\cdot\nabla)\nabla\,p_0+\rho_0\,(\xi\cdot\nabla)\nabla\,\phi_0\;=\;F\,,$$

That is, the vector Green's kernels (depending on the direction) can be obtained from the computation of only two boundary-value problems.

H. Barucq, F. Faucher, D. Fournier, L. Gizon and H. Pham, Efficient computation of modal Green's kernels for vectorial equations in helioseismology under spherical symmetry. Research Report, 2021.

Vector-wave equation with gravity

Comparison with HMI data (white crosses), for $\ell \in (0, 100)$, $\omega/(2\pi) \in (0.5, 4)$mHz.

Including the gravity effect, f and g-modes now appear.

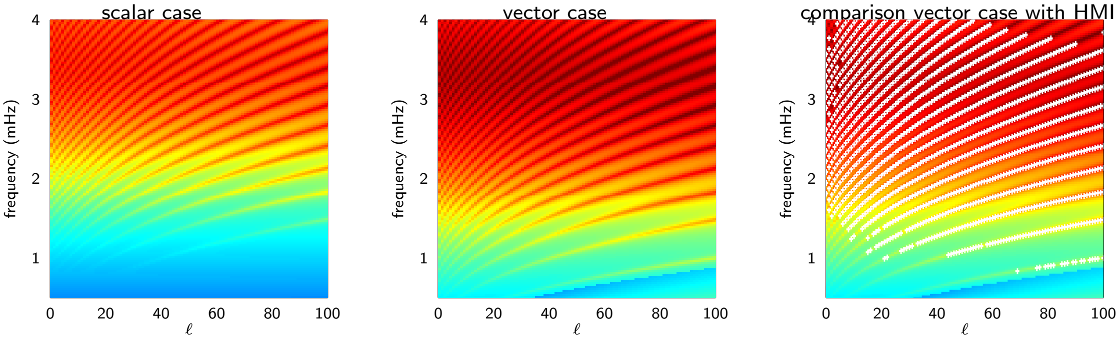

H. Barucq, F. Faucher, D. Fournier, L. Gizon and H. Pham, Efficient computation of modal Green's kernels for vectorial equations in helioseismology under spherical symmetry. Research Report, 2021.

Towards 3D simulations

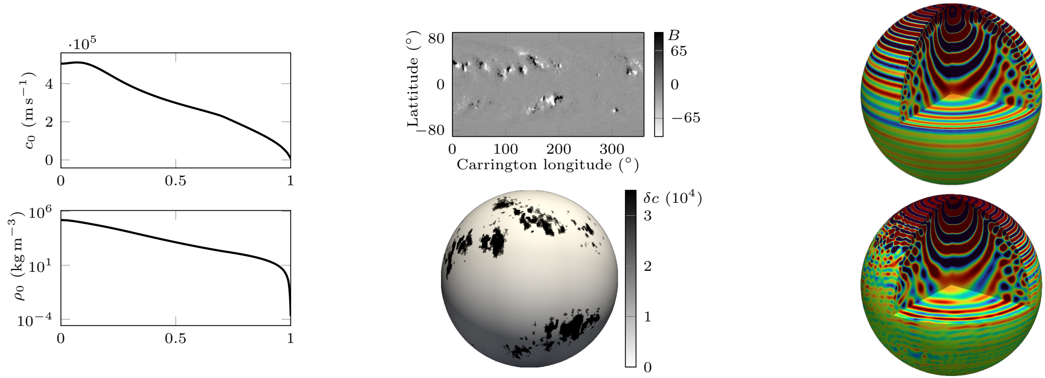

(a) spherical solar background models

(b) Active region as velocity perturbation

(c) Simulations with spherical background (top) and perturbations (bottom).

Scalar-wave propagation in global 3D Sun with in-house code hawen. The memory cost for its factorization is of 3 TiB.

Plan

10 Conclusion

Recap

- Simulation of wave propagation provides a non invasive tool for probing the invisible
- Advanced numerical methods and HPC are mandatory
- Inversion remains very sensitive
- Recovering real data is also very sensitive and mathematical modeling has its part to play

Ongoing works

- Coupling SEM and DG for time-dependent problems in geophysics
- Conducting porous media
- Imaging 3D anisotropic elastic media with new acquisition methods (DAS)
- Solve the 3D Galbrun's equation with and without Cowling's approximation
- Construction of Butterfly diagrams for stars
- and so many very exciting problems

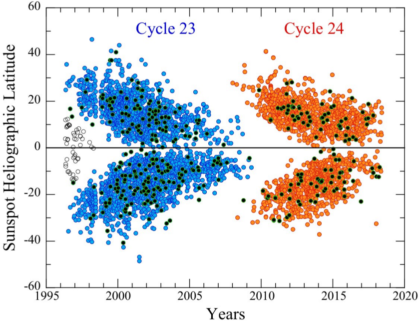

Makutu, September 2022

THANK YOU